First arrival tomography application in low illumination time-lapse reservoir monitoring

Paulo H. B. Alves[1], Roger M. Moreira[1], Marco Cetale[1] and Jorge Lopez[2]

1 - Universidade Federal Fluminense (UFF / PPGDOT / GISIS); 2 - Shell Brasil Petróleo Ltda.

Abstract

We evaluate the classical first arrival tomography applicability in a simple time lapse experiment. A base velocity model is given to generate a small variation to build a monitor model with Santos Basin pre-salt structures. Synthetic base and monitor travel time data is created via eikonal equation solver using a circular shots with Ocean Bottom Nodes. The geometry acquisition employed is formulated specifically for reservoir monitoring with low range of shots and large offsets. A data selection was done to catch only the receiver gathers that contemplate the travel time difference target. The target 4D anomaly difference and the convergence curve is shown. Results show a good 4D anomaly reconstruction at the upper and lower limits of the reservoir. Nevertheless inside it, the reconstruction is not achieved because of the ray tracing kernel limitations.

Introduction

Enhance oil recovery using 4D seismic inversion are been broadly developed to optimize strategically the life range of oil and gas reservoirs. Justice et al. (1989) show a tomography application for this case, but nowadays full waveform inversion has been obtaining the main space in reservoir time lapse velocity model variation (Hicks et al., 2016; Zhou and Lumley, 2021). High defined models can be constructed with elaborate inversion tools (Liu and Gu, 2012), but tomography is a computationally cheap and fast method which may play a relevant role in time lapse studies. Some developments are applied to configure a special geometry acquisition that takes less time to be completed and that is less harmful to the environment. Lopez et al. (2020) presented a circular shot geometry as a tool for target oriented time lapse studies, checking the illumination of seismic rays inside the reservoir using long offsets. Costa et al. (2020) evaluated the refractive waves trajectory via ray tracing in a Santos Basing pre-salt model. Those previous studies needed to modify the velocity model high frequency characteristics because of the ray tracing equations technique limitations Hogan et al. (2007). (Da Silva et al., 2022) checked the model complexity effects applying density properties in seismic modeling using a specific variation of the wave equation for acoustic and isotropic media.

The objective of this study is to check the first arrival seismic tomography availability in target oriented time lapse studies with a circular shot geometry using Ocean Bottom Nodes. The eikonal equation is employed in order to preserve the high contrasted structures built by previous seismic processing inversion steps (Balkaya et al., 2010; Liu and Gu, 2012). Large offsets are considered to foment the refracted waves that propagate inside the reservoir. Although current studies on first arrival tomography are focused on the adjoint-state inversion (Sei and Symes, 1994; Tromp et al., 2005; Taillandier et al., 2009), classical tomography using eikonal equation plus ray tracing is employed (White, 1989; Zhang and Toksöz, 1998; Balkaya et al., 2010).

Theory and Methods

Problems are shown in ray equation solution using strongly heterogeneous velocity models (Cervenỳ, 2001; Hogan et al., 2007; Rawlinson et al., 2008). Because of that, the eikonal equation is employed as a modeling kernel for the first arrival tomography to preserve the base model contrasts. The three-dimensional eikonal equation can be written in the format below

$$(\partial_x T)^2 + (\partial_y T)^2 + (\partial_z T)^2 = s^2, \quad (1)$$

where T and s are the travel time and the slowness volumes respectively. There are a family of methods to solve the eikonal equation. The modern highlights are the fast methods and its improvements such as Fast Marching Method (Sethian, 1996; Rawlinson and Sambridge, 2005; Alton and Mitchell, 2009; Xu et al., 2019; Mirebeau and Portegies, 2019; White et al., 2020), Fast Iterative Method (Jeong and Whitaker, 2008; Dang and Emad, 2014; Hong and Jeong, 2016; Cai et al., 2023) and Fast Sweeping Method (Zhao, 2005, 2007; Bak et al., 2010; Luo and Qian, 2012; Noble et al., 2014; Waheed et al., 2015; Waheed and Alkhalifah, 2017).

Eikonal solver

The formulation of Noble et al. (2014) is used to solve eikonal equation in this work. Solving the equation 1 via finite difference, this solution sweeps the entire domain in eight diferent directions applying operators using specific neighboring points (Zhao, 2005). Accurate travel times are computed due to the eight point operator in its expanded form, initially developed by Vidale (1988) in its truncated form. Although Noble et al. (2014) formulation employs cartesian and spherical coordinates, only cartesian coordinate operators were applied. Some operators were developed based on limitations found in Koketsu (2000) studies. To evaluate the first arrival travel time outside the grid point, a trilinear interpolation is applied at each receiver.

To propagate realistic travel times each grid point has homogeneous velocity and the analytical time is computed in arbitrary source position to start solving the eikonal equation. There is no performance optimization on the eikonal solver and the experiment was concluded using only one computer using the *Xeon E-2286G* processor unit.

4D anomaly construction

Figure 1 illustrates the velocity model of a typical Brazilian pre-salt region, which is employed as our base model. It is assumed that the base model is a good representation of the reservoir, with its top and bottom horizons well established. A monitor model is created by introducing an anomaly due to water injection in the reservoir. A two-dimensional Gaussian function was applied, at the center of the model, slice after slice, increasing 2 % of the velocity between horizons. Decaying is provided by standard deviation in x and y directions assuming the values of 500 m and 1000 m respectively. The model has dimensions x,y,z of 22, 22, 8 km respectively with a fixed spatial discretization of 50 m. Figure 2 shows the difference between the base-monitor models. The target anomaly is quite small, does not exceed 100 m/s, and the classical tomography approach may identify this contrast according with the first arrivals data.

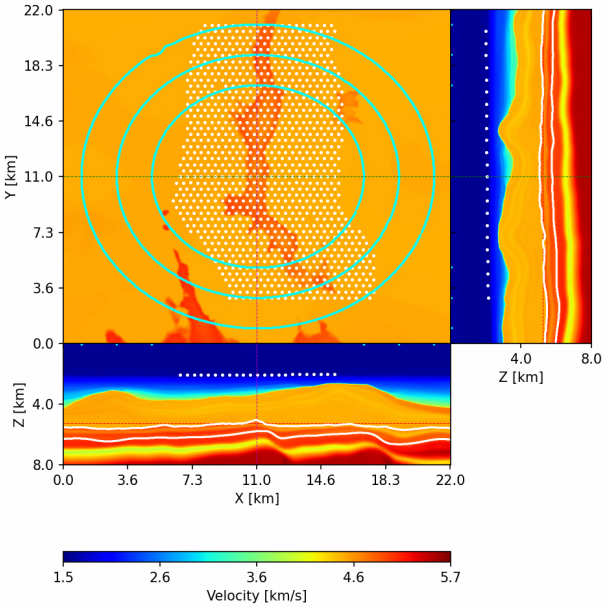

Figure 1: Base model and initial velocity model for the first arrival tomography. Circular shots (cyan) and Ocean Bottom Nodes (white dots) employed to simulate a reservoir (between horizons in white) monitoring acquisition.

The geometry acquisition follow a circular shots design containing 3006 in total and Ocean Bottom Nodes is applied with 1029 in total. The shots and the nodes are spatially spaced between 25 and 400 m each other respectively. The circles offsets are approximately 6, 8 and 10 km from the center of the model and large offsets are presented in simulation, specifically up to 22 km. This geometry is inspired in a real geometry used to acquire seismic data in the Santos Basin - Brazil.

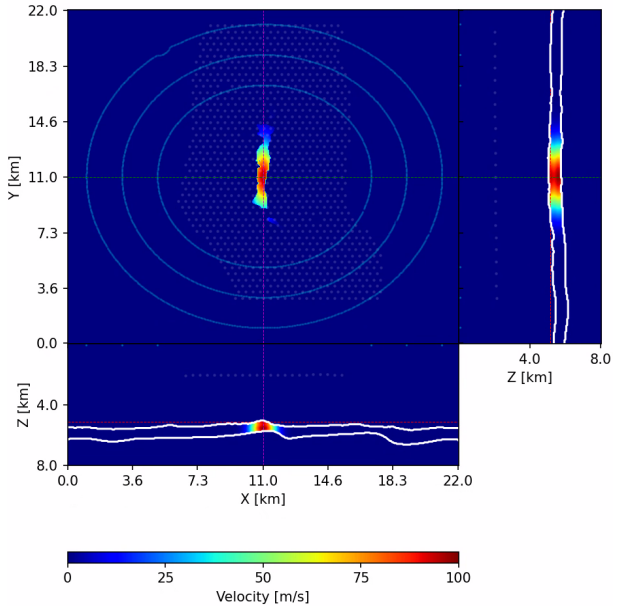

Figure 2: Subtraction of the base and the reference monitor models. 4D anomaly created by a two-dimensional Gaussian function applied between the reservoir horizons limits (white). The target anomaly does not exceed 100 m/s as a result of the 2 % increase in the velocity at the center of the base model.

Data selection

To check the inversion availability, synthetic observed and calculated first arrivals were generated using the base and the monitor models respectively via reciprocity principle. The data difference is obtained to verify the influence of the geometry illumination with respect to the velocity contrasts proposed to recover. Some receiver gathers do not contemplate significant travel time difference, because of that, nodes in the center of the circles were neglected, as shown in Figure 4. This process reduced the execution time of the tomography inversion significantly, as shown in Table 1.

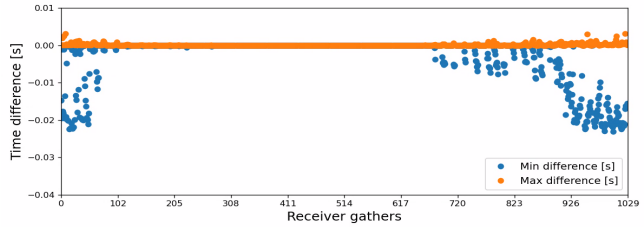

Figure 3: Minimum and maximum difference between synthetic observed and calculated data, generated via reciprocity principle, for each receiver gather. The absolute error is the initial data misfit considered in tomography.

Table 1: Modeling run time for all data and selected data.

	Run time
All data	3 h 21 min 53 s
Selected data	1 h 29 min 56 s

With the decrease of Ocean Bottom Nodes in the acquisition from 1029 to 469, the geometry map changed to just use the largest offsets present. Shortest offsets bring information only from top of the salt when just first arrivals are considered.

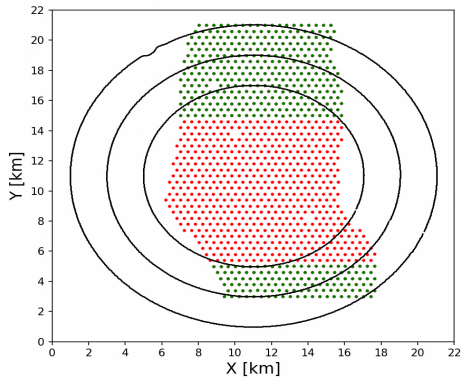

Figure 4: Modified geometry acquisition. Red dots are the nodes neglected, green dots are the nodes used and the black dots are the 3006 shot positions.

Inversion approach

Classical first arrival tomography is used in this work. Although eikonal equation was applied, ray tracing technique was employed to generate the Fréchet derivatives. Ray path was generated using the travel time volume as a function. With the application of the gradient descent method, we can trace ray paths from nodes to source (Vidale, 1988). A non linear inversion and the L_2 norm were applied to minimize the functional below

$$\Phi(\mathbf{m}) = ||\mathbf{d} - \mathbf{G}(\mathbf{m})||_2^2 + \lambda ||\mathbf{L}\mathbf{m}||_2^2 \quad (2)$$

where $\mathbf{d}$ is the observed first arrival data, $\mathbf{G}(\mathbf{m})$ is the calculated first arrival data for the current model $\mathbf{m}$, λ is the regularization parameter and $\mathbf{L}$ is a discrete derivative operator. In this work $\mathbf{L}$ works as Tikhonov regularization in the form of the second order derivative operator to stabilize the inversion scheme. Bulhões et al. (2021) show that second order Tikhonov regularization has fast convergence in first arrival tomography.

A linear system is solved at each tomography iteration. To avoid matrix inversion, the least square problem was solved applying a special type of conjugate gradient method that compute solution of $Ax = b$ without computing the Hessian matrix (Hestenes et al., 1952). So, the problem we need to solve iteratively is given by

$$\mathbf{A}^T\mathbf{A}\,\Delta\mathbf{m} = \mathbf{A}^T\Delta\mathbf{d} \quad (3)$$

where $\mathbf{A}$ is the composition of the Fréchet derivatives with the second order Tikhonov regularization operator, $\Delta\mathbf{m}$ is the slowness model variation and $\Delta\mathbf{d}$ is the difference of the observed with the calculated data. Inversion objects formulated explicitly follow the scheme

$$\mathbf{A} = \begin{bmatrix} \mathbf{G_i} \\ \mathbf{L} \end{bmatrix}; \quad \Delta\mathbf{d} = \begin{bmatrix} \mathbf{d}^{\text{obs}} - \mathbf{d}_i^{\text{cal}} \\ \vec{0} \end{bmatrix}; \quad \Delta\mathbf{m} = \mathbf{m}_{i+1} - \mathbf{m}_i, \quad (4)$$

where $\mathbf{G}_i$ is a matrix containing the length of rays per inversion grid cell at iteration i, $\mathbf{L}$ is a second order Tikhonov derivative operator with $\lambda = 0.1$, $\mathbf{d}^{\text{obs}}$ is the observed data, $\mathbf{d}_i^{\text{cal}}$ is the calculated data in current model $\mathbf{m}_i$ and $\mathbf{m}_{i+1}$ is the model update at each iteration.

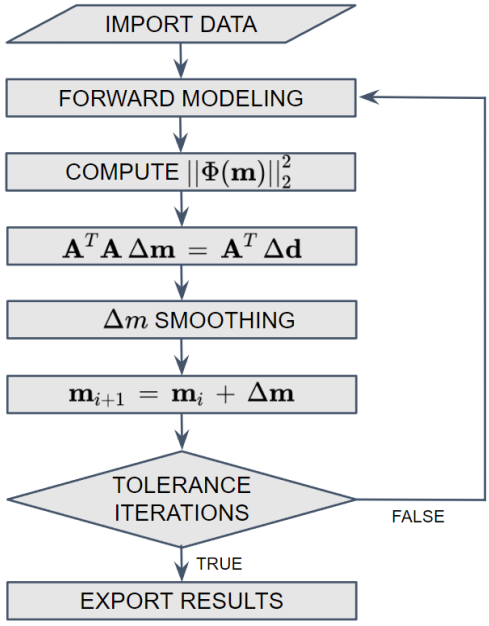

Figure 5: Classical tomography inversion flowchart.

The convergence criterion can be assigned by a tolerance term or with a total number of iterations. In this work 10 iterations were necessary to a satisfactory model reconstruction and the tolerance criterion was not needed. Sparse matrix storage using coordinate lists was applied to reduce computationally the problem. The least square conjugate gradient solved the sparse problem in equation 3 with no more than 8 iterations. Between tomography iterations, a Gaussian smoothing filter, with standard deviation equal to 2 and 15 samples, was applied in slowness variation to reduce artifacts caused by the low illumination characteristics. The full workflow of tomography inversion can be better visualized in Figure 5, where the results are the convergence curve with the objective function norm and the recovered model at each iteration.

Results and Discussions

The 4D anomaly recovered at the final iteration is presented in Figure 6, overlayed with geometry acquisition and the reservoir limits. This difference shows the high influence of ray tracing and the model update preferred regions inside the reservoir. All the slices are cutting the model at the same positions. First, the 4D anomaly recovered presents noise artifacts outside the reservoir, inclusively on top of the salt. That is because the illumination favoring the top of the salt and some noise was expected to appear in this region. On the other hand, noise amplitude is well below the target anomaly. Second, with the refined grid inversion used (the same grid spacing than the model, i.e. 50 m), the 4D anomaly recovered presents reconstruction just near of the reservoir limit interfaces. This characteristic is intrinsic in the modeling using the ray tracing combined with the eikonal equation, where the ray

paths are thin and the propagation waves prefer surfaces.

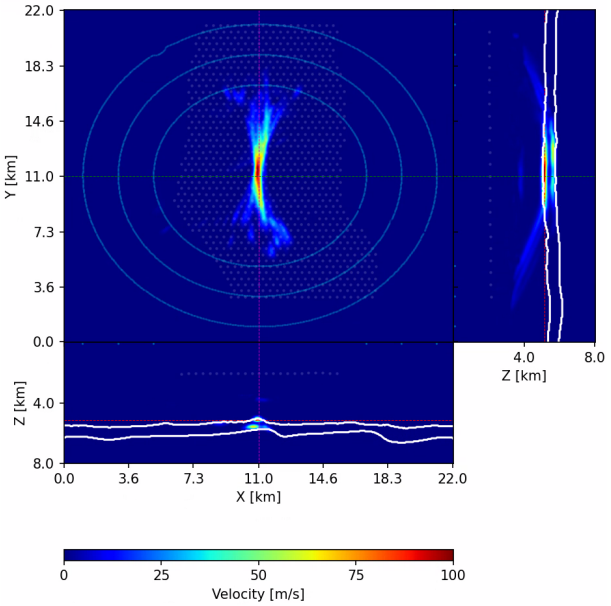

Figure 6: 4D anomaly reconstructed as a result of the first arrival tomography. Reservoir limits marked with solid white line. Geometry acquisition with opacity, shots in cyan and nodes in white dots.

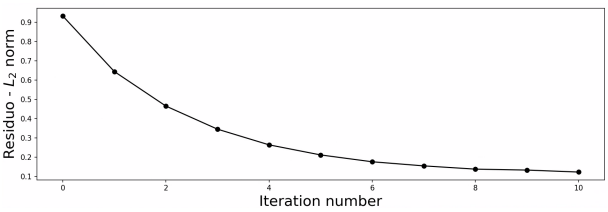

Figure 7: Convergence curve for the experiment.

As a result of the ray tracing kernel, the resolution of the recovered model depends on the inversion grid refinement, but the high velocity contrasts were conserved because of eikonal equation usage. If the mesh were coarser, the inversion would recover the velocities inside the reservoir, but the recovered velocities would not respect the reservoir limits, exceeding the limits both up and down. Total inversion took 15 h 52 min 31 s to complete and the convergence curve is presented in Figure 7. The objective function L_2 norm is small since the inversion beginning. We have a reference and a recovered 4D anomaly, so the difference of these anomaly can be found in Figure 8. With this analysis is possible to measure the wrong 4D anomaly reconstruction and this makes evident the non-reconstruction in the center of the reservoir, but only in the upper and lower limits. These characteristics are clear in the projections of the model in ZY and ZX planes. The noise artifacts outside the reservoir round between 5 to 15 m/s, the maximum and minimum error are 84.5 and -90.3 m/s respectively, the mean error is -0.015 m/s and the standard deviation is 1.45 in all 4D difference volume. The data after inversion was represented in Figure 9, just for the nodes considered in inversion. The inversion reduced the data misfit from 0.015 to 0.003 s on absolute average, comparing with the Figure 3 at the same time scale.

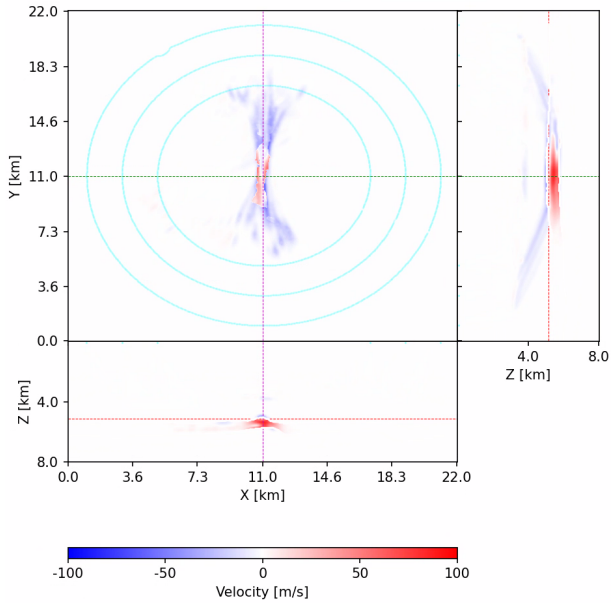

Figure 8: 4D anomaly difference obtained from the subtraction of the reference with the recovered anomaly.

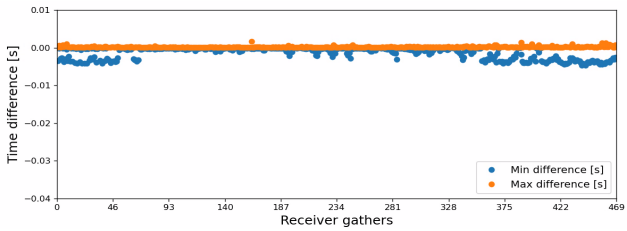

Figure 9: Travel time difference at each receiver gather only using the selected nodes. Data generated with the 10th iteration recovered model.

Conclusion

The classical first arrival tomography can bring information of small velocity contrasts at the reservoir limits without change the base model significantly, but not inside the reservoir completely due to the refracted waves tendency propagation at the layer interfaces. The method obtained fast convergence without distinguished noise and the recovered anomaly respected the velocity range of the known anomaly. The significant model update, in the ideal case, is only on the refractive interfaces. The target oriented geometry acquisition scheme brought reservoir illumination, but not enough for classical tomography using eikonal plus ray tracing kernels. The way to update inside the reservoir is to generate a coarser grid inversion, but it would imply in a low resolution recovered model where the update velocities would exceed both limits of the reservoir. The adjoint-state tomography might be more suitable for this low illumination case, due to the non-use of ray tracing kernels. It could bring more information inside the reservoir because it use total information of the eikonal equation.

References

Alton, K., and Mitchell, I. M., 2009, Fast marching methods for stationary hamilton–jacobi equations with axis-aligned anisotropy: SIAM Journal on Numerical Analysis, **47**, no. 1, 363–385.

Bak, S., McLaughlin, J., and Renzi, D., 2010, Some improvements for the fast sweeping method: SIAM Journal on Scientific Computing, **32**, no. 5, 2853–2874.

Balkaya, Ç., Akçığ, Z., and Göktürkler, G., 2010, A comparison of two traveltime tomography schemes for crosshole radar data: Eikonal-equation-based inversion versus ray-based inversion: Journal of Environmental & Engineering Geophysics, **15**, no. 4, 203–218.

Bulhões, F. C., Santos, M. A. C., Santos, L. A., and de Almeida, V. X. T., 2021, Regularization effects on 2d seismic refraction tomography: case study on shallow marine environment: 17th International Congress of the Brazilian Geophysical Society.

Cai, W., Zhu, P., and Li, G., 2023, Improved fast iterative method for higher calculation accuracy of traveltimes: Computers & Geosciences, page 105331.

Cervenỳ, V., 2001, Seismic ray theory:, volume 110 Cambridge university press Cambridge.

Costa, F., Capuzzo, F., de Souza Jr, A., Moreira, R., Lopez, J., and Cetale, M., 2020, Understanding refracted wave paths for brazilian pre-salt target-oriented imaging: SEG Technical Program Expanded Abstracts 2020, 2375–2380.

Da Silva, S., Karsou, A., Moreira, R., Lopez, J., and Cetale, M., 2022, Klein-gordon equation and variable density effects on acoustic wave propagation in brazilian pre-salt fields: Klein-gordon equation and variable density effects on acoustic wave propagation in brazilian pre-salt fields:, 83rd EAGE Annual Conference & Exhibition, 1–5.

Dang, F., and Emad, N., 2014, Fast iterative method in solving eikonal equations: a multi-level parallel approach: Procedia Computer Science, **29**, 1859–1869.

Hestenes, M. R., Stiefel, E., , et al., 1952, Methods of conjugate gradients for solving linear systems: Journal of research of the National Bureau of Standards, **49**, no. 6, 409–436.

Hicks, E., Hoeber, H., Houbiers, M., Lescoffit, S. P., Ratcliffe, A., and Vinje, V., 2016, Time-lapse full-waveform inversion as a reservoir-monitoring tool—a north sea case study: The Leading Edge, **35**, no. 10, 850–858.

Hogan, C. M., Margrave, G. F., , et al., 2007, Ray-tracing and eikonal solutions for low-frequency wavefields: CREWES Research Report, **19**.

Hong, S., and Jeong, W.-K., 2016, A multi-gpu fast iterative method for eikonal equations using on-the-fly adaptive domain decomposition: Procedia Computer Science, **80**, 190–200.

Jeong, W.-K., and Whitaker, R. T., 2008, A fast iterative method for eikonal equations: SIAM Journal on Scientific Computing, **30**, no. 5, 2512–2534.

Justice, J., Vassiliou, A., Singh, S., Logel, J., Hansen, P., Hall, B., Hutt, P., and Solanki, J., 1989, Acoustic tomography for monitoring enhanced oil recovery: The Leading Edge, **8**, no. 2, 12–19.

Koketsu, K., 2000, Finite difference traveltime calculation for head waves travelling along an irregular interface: Geophysical Journal International, **143**, no. 3, 729–734.

Liu, Q., and Gu, Y., 2012, Seismic imaging: From classical to adjoint tomography: Tectonophysics, **566**, 31–66.

Lopez, J., Neto, F., Cabrera, M., Cooke, S., Grandi, S., and Roehl, D., 2020, Refraction seismic for pre-salt reservoir characterization and monitoring: SEG International Exposition and Annual Meeting.

Luo, S., and Qian, J., 2012, Fast sweeping methods for factored anisotropic eikonal equations: multiplicative and additive factors: Journal of Scientific Computing, **52**, no. 2, 360–382.

Mirebeau, J.-M., and Portegies, J., 2019, Hamiltonian fast marching: a numerical solver for anisotropic and non-holonomic eikonal pdes: Image processing on line, **9**, 47–93.

Noble, M., Gesret, A., and Belayouni, N., 2014, Accurate 3-d finite difference computation of traveltimes in strongly heterogeneous media: Geophysical Journal International, **199**, no. 3, 1572–1585.

Rawlinson, N., and Sambridge, M., 2005, The fast marching method: an effective tool for tomographic imaging and tracking multiple phases in complex layered media: Exploration Geophysics, **36**, no. 4, 341–350.

Rawlinson, N., Hauser, J., and Sambridge, M., 2008, Seismic ray tracing and wavefront tracking in laterally heterogeneous media: Advances in geophysics, **49**, 203–273.

Sei, A., and Symes, W. W., 1994, Gradient calculation of the traveltime cost function without ray tracing: SEG Technical Program Expanded Abstracts 1994, 1351–1354.

Sethian, J. A., 1996, A fast marching level set method for monotonically advancing fronts.: Proceedings of the National Academy of Sciences, **93**, no. 4, 1591–1595.

Taillandier, C., Noble, M., Chauris, H., and Calandra, H., 2009, First-arrival traveltime tomography based on the adjoint-state method: Geophysics, **74**, no. 6, WCB1–WCB10.

Tromp, J., Tape, C., and Liu, Q., 2005, Seismic tomography, adjoint methods, time reversal and banana-doughnut kernels: Geophysical Journal International, **160**, no. 1, 195–216.

Vidale, J., 1988, Finite-difference calculation of travel times: Bulletin of the seismological society of America, **78**, no. 6, 2062–2076.

Waheed, U. b., and Alkhalifah, T., 2017, A fast sweeping algorithm for accurate solution of the tilted transversely isotropic eikonal equation using factorization: Geophysics, **82**, no. 6, WB1–WB8.

Waheed, U. B., Yarman, C. E., and Flagg, G., 2015, An iterative, fast-sweeping-based eikonal solver for 3d tilted anisotropic media: Geophysics, **80**, no. 3, C49–C58.

White, M. C., Fang, H., Nakata, N., and Ben-Zion, Y., 2020, Pykonal: a python package for solving the eikonal equation in spherical and cartesian coordinates using the fast marching method: Seismological Research Letters, **91**, no. 4, 2378–2389.

White, D., 1989, Two-dimensional seismic refraction tomography: Geophysical Journal International, **97**, no. 2, 223–245.

Xu, J., Chen, Y., Yang, X., and Zhang, M., 2019, Fast marching-based path generating algorithm in anisotropic environment with perturbations: IEEE Access, **8**, 5256–5263.

Zhang, J., and Toksöz, M. N., 1998, Nonlinear refraction traveltime tomography: Geophysics, **63**, no. 5, 1726–1737.

Zhao, H., 2005, A fast sweeping method for eikonal equations: Mathematics of computation, **74**, no. 250, 603–627.

Zhao, H., 2007, Parallel implementations of the fast sweeping method: Journal of Computational Mathematics, pages 421–429.

Zhou, W., and Lumley, D., 2021, Nonrepeatability effects on time-lapse 4d seismic full-waveform inversion for ocean-bottom node datanr effects on 4d fwi: Geophysics, **86**, no. 4, R547–R561.

Acknowledgments

The authors from Fluminense Federal University (UFF) gratefully acknowledge support from Shell Brasil Petróleo Ltda through the RD "Refraction seismic for pre-salt reservoirs" (ANP no. 21727-3.) project at UFF and the strategic importance of the support given by National Agency for Petroleum (ANP) through the RD levy regulation. Authors would like to thank the Seismic Imaging and Seismic Inversion Group (GISIS) team for all knowledge shared and also would like to thank UFF and Oceans and Land Dynamics graduate program (PPGDOT) for the all infrastructure to develop this work. Also, the authors would like to thank Rodrigo S. Stern (UFF/GISIS) for the crucial IT support.